

# Sinkholes and uvalas in evaporite karst: spatio-temporal development with links to base-level fall on the eastern shore of the Dead Sea

Robert A. Watson<sup>1\*</sup>, Eoghan P. Holohan<sup>1</sup>, Djamil Al-Halbouni<sup>2</sup>, Leila Saberi<sup>3</sup>, Ali Sawarieh<sup>4</sup>, Damien Closson<sup>5</sup>, Hussam Alrshdan<sup>4</sup>, Najib Abou Karaki<sup>6+</sup>, Christian Siebert<sup>7</sup>, Thomas R. Walter<sup>2</sup>, & Torsten Dahm<sup>2</sup>

<sup>1</sup> UCD School of Earth Sciences, University College Dublin, Dublin, Ireland

\* Now at Department of Earth Sciences, University of Graz, A-8010 Graz, Austria

<sup>2</sup> Helmholtz Centre Potsdam (GFZ), Section 2.1, Potsdam, Germany

<sup>3</sup> University of Minnesota, Department of Earth Sciences, Minneapolis, USA

<sup>4</sup> Ministry of Energy & Mineral Resources, Amman, Jordan

<sup>5</sup> Geographic Information Management, Leuven, Belgium

<sup>6</sup> Department of Environmental and Applied Geology, University of Jordan, Amman, 11942, Jordan

+ On sabbatical leave at the Environmental Engineering Department, Al-Hussein bin Talal University, Ma'an-Jordan

<sup>7</sup> Helmholtz Centre for Environmental Research – UFZ, T. Lieser Str. 4, Halle 06120, Germany

*Correspondence to:* Robert A. Watson (robert.watson@uni-graz.at)

**Abstract.** Enclosed topographic depressions are characteristic of karst landscapes on Earth. The developmental relationship between depression types, such as sinkholes (dolines) and uvalas, has been subject of debate, mainly because the long developmental timescales in classical limestone karst settings impede direct observation. Here we characterise the morphometric properties and spatio-temporal development of >1100 sinkholes and five uvalas formed from ~1980 to 2017 in an evaporite karst setting along the eastern coast of the hypersaline Dead Sea (at Ghor Al-Haditha, Jordan). The development of sinkhole populations and individual uvalas is intertwined in terms of onset, evolution and cessation. Many sinkholes develop initially in clusters; the uvalas develop as a larger-scale, gentler and structurally-distinct depressions around such clusters. The uvalas do not form by coalescence of sinkholes. The location of new sinkholes and uvalas shows a marked shoreline-parallel migration with time, followed by a marked shoreline-perpendicular (i.e. seaward) growth with time. These observations are consistent with theoretical predictions of karstification controlled by a laterally-migrating interface between saturated/under-saturated groundwater, as induced by the 35 m fall in the Dead Sea level since 1967.

More generally, our observations indicate that uvalas and the sinkhole populations within them, although morphometrically distinct, can develop near-synchronously by subsidence in response to sub-surface erosion.

## 1 Introduction

35 Sinkholes (also termed ‘dolines’) and uvalas are types of enclosed topographic depression, and they are characteristic of karst regions. In limestone karst areas, where uvalas have been first and most extensively described, differences between these depression types occur in regard to scale, inter-relationship and morphometry (Ćalić, 2011). Uvalas typically occur on a larger scale than dolines; uvala diameters in limestone karst are typically 1000-5000 m (Ćalić, 2011), whereas sinkhole diameters in limestone karst  
40 are sub-kilometre and typically in the range of 10-200 m (Bondesan et al., 1992). A single uvala typically includes numerous dolines within it. Morphometrically, uvalas commonly have lower slope inclinations and more complex shapes than dolines, both in plan-view and in three-dimensions (Ćalić, 2011). Additionally, uvalas are regarded as distinct from another type of enclosed karstic depression, a polje. Compared to uvalas, poljes in limestone karst occur on still-larger scales, from a several km<sup>2</sup> to several  
45 hundred km<sup>2</sup> in size (Kranjc, 2013). Poljes also typically have steeper sides, are elongated in plan-view, and have characteristically wide and flat bottoms.

Historically, there has been considerable debate over the process(es) of uvala formation, and over the genetic relationship between uvalas and sinkholes (dolines), in limestone karst areas (see (Ćalić, 2011)  
50 for summary). Various mechanisms proposed for the formation of uvalas include areally-distributed surface dissolution, sub-surface mass-wasting (corrosion) and coalescence of sinkholes. Cvijić (1926) proposed that sinkholes evolve by coalescence into uvalas and ultimately into poljes (a cyclical karst evolution), but many authors since have considered this concept to be problematic (Ćalić, 2011; Sauro, 2012). Nonetheless, the term uvala has been regarded by many authors as synonymous with ‘compound  
55 sinkhole’, ‘nested sinkhole’ and ‘valley sink’ (cf. Monroe, 1970).

The main problem for unravelling the spatio-temporal relationships between uvala and sinkhole (dolines) development in limestone karst areas is that the landform evolution is controlled by the relatively slow dissolution kinetics of carbonate minerals. Consequently, the development of these landform types is not directly observable in such areas. Furthermore, the slow rate of karstic processes means that limestone areas are susceptible also to long-term geomorphic influences from changing climate and active tectonics. Indeed, the areas in which such uvalas and dolines have been best documented occur in tectonically complex settings in which climate has varied considerably over time, such that many landforms have been modified not only by karst processes but also by fluvial and/or glacial processes.

An opportunity to shed new light on the geometric and genetic relationships between sinkholes and uvalas has arisen with their rapid development in an evaporite karst setting over the last 35 years at the margins of the hypersaline Dead Sea (Arkin and Gilat, 2000; Taqieddin et al., 2000; Yechieli et al., 2006; Avni et al., 2016; Abelson et al., 2017). The sinkholes, which have been the focus of previous work, now number in the several thousands. They represent a substantial geohazard in the Dead Sea region, and they have already destroyed or damaged several tourism facilities, factories, evaporation pond dykes, highways, link roads, houses and farmland. Although the occurrence of uvala-like depressions has also been documented in areas of evaporite karst such as the Dead Sea (Al-Halbouni et al., 2017; Avni et al., 2016; Baer et al., 2002; Closson, 2005; Frumkin, 2013), the central uplands of Turkey (Doğan, 2005; Doğan and Özel, 2005; Waltham, 2015) and areas of Saudi Arabia (Gutiérrez and Cooper, 2013; Youssef et al., 2015), they have not been studied as extensively as their carbonate equivalents.

The Dead Sea level represents the regional hydrological base-level, and its largely anthropogenically-forced decline at a gradually increasing rate since the late 1960s (Lensky et al., 2005) has been linked with the sinkhole formation. In theory, the base-level fall should cause a seaward shift of the ‘fresh-saline interface’ developed between the hypersaline Dead Sea brine and less saline (i.e. relatively ‘fresh’) groundwater (Salameh and El-Naser, 2000; Yechieli, 2000; Yechieli et al., 2009). Such a shift should enable groundwater under-saturated with respect to halite and other evaporitic minerals to infiltrate the evaporite deposits in the subsurface, thus triggering karstification and surface subsidence. The location

85 of karstification and sinkhole formation is controlled by the intersection of the ‘fresh-saline interface’ with the shoreward edge of evaporite deposits in the sub-surface. A prediction of this theory is that new sinkhole development should shift seaward with time also. Evidence for such a shift on the well-studied western Dead Sea shore is somewhat patchy (Abelson et al., 2017; Avni et al., 2016), however, and it has been regarded by some authors as unconvincing (Charrach, 2018). Preferential flow of relatively fresh  
90 groundwater into evaporite-rich deposits along conductive regional tectonic faults has been proposed as an alternative control on the location of sinkhole (and uvala) development (Abelson et al., 2003; Charrach, 2018; Closson, 2005; Shalev et al., 2006).

In this paper, we provide a first detailed documentation of the spatio-temporal evolution of sinkholes and uvalas on the eastern shore of the Dead Sea, at Ghor Al-Haditha in Jordan. Our aims are to discern spatio-temporal inter-relationship of these two types of karstic depression, and to examine how their  
95 development relates to base-level fall. Our approach combines remote sensing data spanning the 50 year duration of base-level fall from 1967-2017 with close-range photogrammetric surveys and field observations made in 2014-2017. Our results show the most detailed insights to date into the spatio-temporal development of sinkholes and uvalas in evaporite karst settings, and the clearest yet illustration  
100 the effect of base-level fall on that development. Our study’s overall aim is to contribute these fresh insights to the ongoing debate about the nature and origin of uvalas and about their relationship to the sinkholes within them.

## 2 Tectonic and hydro-geological framework

The Dead Sea is the hyper-saline terminal lake of the Jordan River (Figure 1A), and it lies within the  
105 ~150 km long and ~8-15 km wide Dead Sea basin (Garfunkel and Ben-Avraham, 1996). The basin lies at a left step (or bend) along the left-lateral Dead Sea Transform fault system. Maximum tectonic subsidence is ~8.5 km around the Lisan peninsula, adjacent to our study area (Ten Brink and Flores, 2012). The basin has subsided rapidly from the late Pliocene to present (Ten Brink and Flores, 2012), and in that time has hosted several palaeo-lakes of varying size and duration (Bartov et al., 2002; Torfstein et al., 2009). With  
110 respect to modern global mean sea level (msl), a high-stand of -162 m msl was reached at around 25 ka



ago, during the 'Lisan Lake' episode. The modern Dead Sea initiated after a major low-stand at around 10 ka (Bartov et al., 2002). As its level has declined from -395 m msl to -431 m msl (1967-2017), the modern lake has divided into northern and southern parts; the latter is now occupied entirely by industrial salt evaporation ponds. The base level fell at a rate of 0.5 m yr<sup>-1</sup> in the 1970's, and at a rate of 1.1 m yr<sup>-1</sup> in the last decade. In absolute terms, the lake level has declined by 37 m as of 2017 and is forecast to drop a further 25-70 m by 2100 (Asmar and Ergenzinger, 2002; Yechieli and Gavrieli, 1998).

The Ghor Al-Haditha study area, which is about 25 km<sup>2</sup> in size, is situated on the southeast shore of the northern part of the Dead Sea (**Figure 1A**). The area lies in a zone of tectonic complexity at the eastern basin margin, where subsidence is relayed between several major tectonic structures. From south to north, these are: the N24°-trending Wadi Araba fault; the N0°-trending Ghor Safi fault; the Ed-Dhira monoclinical flexure; and the N80°-trending Siwaqa fault. Further north again, and marking the north-east boundary of the study area, is a prominent N0°-trending escarpment (**Figure 1B**). This probably reflects the orientation of another major basin-bounding fault (Khalil, 1992), here termed the Eastern Boundary Fault (**Figure 1C**; cf. Meqbel et al., 2013), although the exact location of the fault trace is unclear. Three major *wadi* (dry river valley) systems, Wadi Ibn Hammad, Wadi Mutayl and Wadi al Mazra'a (the latter lies just outside the study area to the southwest) drain the uplands to the east and southeast. These wadi systems have formed an alluvial fan plain at elevations between -360m and -380m in the south of the study area (**Figure 1B**). Smaller alluvial fans occur sporadically along the coastline in the central and northern parts of the study area. West and north of the alluvial plain, exposure of the former lakebed by the ongoing recession of the Dead Sea has formed a 'mud-flat' or 'salt-flat'. At the transition between the two lithologies, numerous artesian springs are found, which feed surface streams that drain into the Dead Sea via numerous channels. Other surface stream channels in the study area lack these groundwater-fed springs and are instead fed by water drained from the various wadi systems during flood events.

The geology of the Ghor Al-Haditha study area (**Figure 1C**) comprises folded and faulted sequences of siliciclastic or carbonate rocks, which are locally overlain by semi-consolidated to unconsolidated lacustrine or alluvial deposits (Khalil, 1992). Hydrogeologically, there are three principal aquifer units:

(1) a lower sandstone aquifer comprising the Ram group and Kurnub formation of Cambrian to early  
140 Cretaceous ages, respectively; (2) an upper carbonate aquifer spanning the Ajlun and Belqa groups of late  
Cretaceous to early Tertiary age; and (3) a superficial aquifer in the Lisan formation of Plio-Pleistocene  
age (Khalil, 1992). The Lisan formation comprises both alluvial and lacustrine deposits. The alluvium  
consists of poorly-sorted, semi-consolidated to unconsolidated sands and gravels interbedded with minor  
145 silts and clays (El-Isa et al., 1995; Sawarieh et al., 2000). Similar, stratigraphically younger, but  
unconsolidated alluvial deposits are probably equivalent to the Ze'elim formation of Holocene age (Abou-  
Karaki et al., 2016). The Lisan and Ze'elim formations also comprise lacustrine deposits, some of which  
are exposed on the former Dead Sea bed. These comprise laminated to thinly bedded layers of marl, clay,  
evaporites and silt interbedded with a spatially variable proportion of distributed lenses or layers of  
evaporites such as halite, aragonite and gypsum (Arkin and Gilat, 2000; Polom et al., 2018). Similar  
150 lacustrine deposits likely extend **in** under the alluvial fan plain (Polom et al., 2018).

**Figure 1 (page 7): overview of the Ghor Al-Haditha study area. (A) Advanced Land Observing Satellite (ALOS) 30m Digital Surface Model (DSM) of the Dead Sea study area, showing the regional tectonic regime. WBF: Western Boundary Fault; SiF: Siwaqa Fault; LD: Lisan Diapir; EDF: Ed Dhira Flexure; GSF: Ghor Safi Fault; SD: Sedom Diapir; SeF: Sedom Fault; WAF: Wadi Araba Fault. (B) ALOS 30m DSM showing relief in the study area, as highlighted in red in (A), along with the footprints of the 2014, 2015 and 2016 drone and field surveys. The flowpaths of the Wadi Mutayl and Wadi Ibn Hamad are shown, along with the positions of the regional Dead Sea Highway and the village of Ghor Al-Haditha. (C) Simplified geological map of the study area, partly based on 1:50,000 scale mapping of Jordanian Ministry of Energy and Mineral Resources (Khalil, 1992) and partly on our own work. The stratigraphy generally dips acutely to the southeast, while striking to the northeast. Also shown is the right-lateral oblique Siwaqa fault, the inferred position of the Eastern Boundary Fault (down-throwing to the east), and the axis of the Haditha syncline. The two boreholes of El-Isa et al. (1995) are labelled 'BH1' and BH2'. The red ~~and black~~ star indicates the position of the Numeira Mud Factory, which is now **defunct** after being destroyed by sinkhole formation at the site.**

155  
160

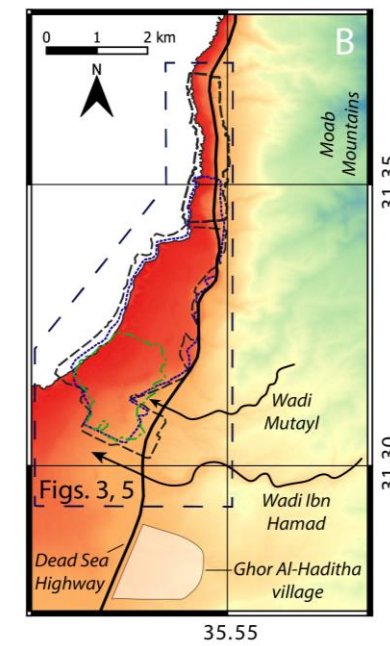
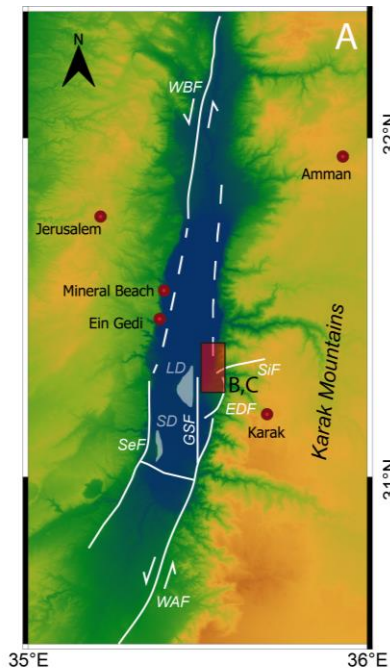


Figure 1A

Elevation [m]

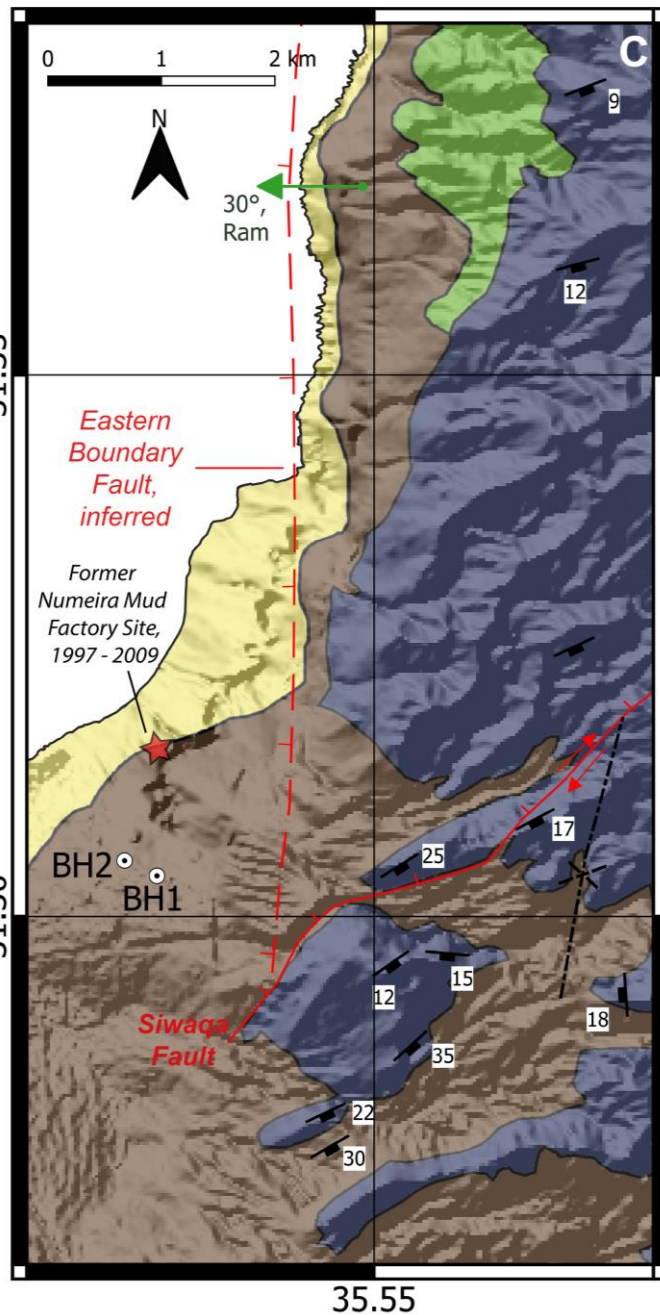
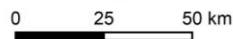
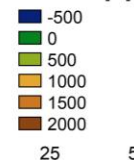


Figure 1B

Elevation [m]

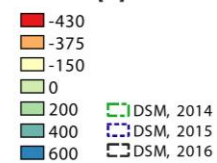
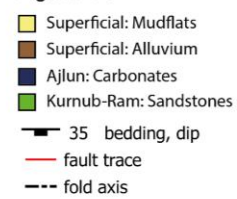


Figure 1C



### 165 3 Data and Methods

Our data set includes high resolution optical satellite imagery and aerial survey photographs covering the 50-year period from 1967-2017 (**Table 1**). We orthorectified and pansharpened the satellite imagery by using standard algorithms and workflows in the PCI Geomatica software package. For orthorectification of the 2002-2010, 2011-2013 and 2014-2015 satellite imagery, we used the Shuttle Radar Topography Mission (SRTM) Digital Elevation Model (DEM), the Advanced Spaceborne Thermal Emission and Reflection Radiometer (ASTER) DEM, and the Advanced Land Observing Satellite (ALOS) World 3D Digital Surface Model (DSM), respectively. For the Pleiades images from 2016 and 2017, atmospheric correction, orthorectification and georeferencing were conducted by Airbus against the Astrium Elevation 30 global DEM. All pre-2016 images were georeferenced by using nine Ground Control Points (GCPs) with accuracies of  $\pm 0.71\text{m}$ , which were collected in 2015 using a Trimble XRTpro dual-frequency GPS receiver with real-time corrections (RTK). Additional co-registration of pre-2016 imagery was performed with respect to the 2017 Pleiades imagery by using tools from the GDAL/OGR library (GDAL/OGR Contributors, 2018) with numerous manually-selected tie-points. In the case of the 1967 image, the use of ESRI online World Imagery was also necessary for further co-registration due to the geographical limits of the 2017 Pleiades imagery. For all satellite imagery metadata and a full error analysis please refer to the Supplementary Material.

Close-range photogrammetric surveys undertaken in October 2014, October 2015 and December 2016 provide yet higher resolution orthophoto mosaics and DSMs (for survey limits, see **Figure 2B**). The surveyed areas were imaged from a helikite or drone at a height of  $\sim 100\text{ m}$  with a 16 Megapixel (MP) Ricoh GR camera (2014), a 12 MP GoPro Hero4 camera with modified lens (2015) or with a 12 MP DJI Phantom 3 inbuilt camera (2016). During each survey, 50-60 temporary GCPs were measured with a Trimble ProXRT differential GPS receiver with RTK. Al-Halbouni et al. (2017) detail the procedure for generating these orthophoto mosaics and DSMs. The internal horizontal and vertical uncertainty of the DSMs is estimated to be: 2014 (10 cm, 11 cm), 2015 (12, 17 cm) and 2016 (37, 31 cm).



All data were integrated and analysed within a Geographic Information System (GIS) software package (Q-GIS). The number and extent of remotely-sensed sinkholes represent minima, as local farmers have filled in sinkholes to mitigate disruption to their work. Therefore, we also include information from sources that undertook earlier field surveys in communication with local farmers (El-Isa et al., 1995; Sawarieh et al., 2000; Closson and Abou-Karaki, 2009). Using historical measurements of the Dead Sea level from the Israel Marine Data Center ( ISRAMAR; Israel Oceanographic and Limnological Research - Israel Marine Data Center, 2017) and the Jordanian Ministry of Water and Irrigation (MWI; El-Isa et al., 1995), we reconstructed the former Dead Sea bathymetry in the study. The shoreline was digitised from each satellite or aerial image (**Figure 2**), and the level of the Dead Sea for the year of image acquisition was assigned to it, such that each shoreline represented a bathymetric contour. A linearly interpolated raster of bathymetric contours with a resolution of 23m was then generated by using inverse distance weighting (**Figure 3**). The 2016 DSM was then down-sampled to the same resolution and the difference of the two relief models was calculated (bathymetric contours – 2016 DSM). For a table of the Dead Sea level data used please refer to the Supplementary Material.

	Data Source	Aquisition Year(s)	Resolution (m/pix)
Optical Satellites	Corona	1967, 1968, 1970	2.0
	Quickbird	2002, 2004-2007, 2012	0.6
	Ikonos	2006	0.8
	Worldview 1	2008, 2011, 2012	0.5
	GeoEye-1	2009-2010	0.5
	Worldview 3	2014	0.3
	Pleiades 1a	2013, 2015 - 2017	0.5
Aerial Surveys	RJGC Aerial	1981, 1992, 2000	0.6
	Drone and Helikite surveys	2014 - 2016	0.1

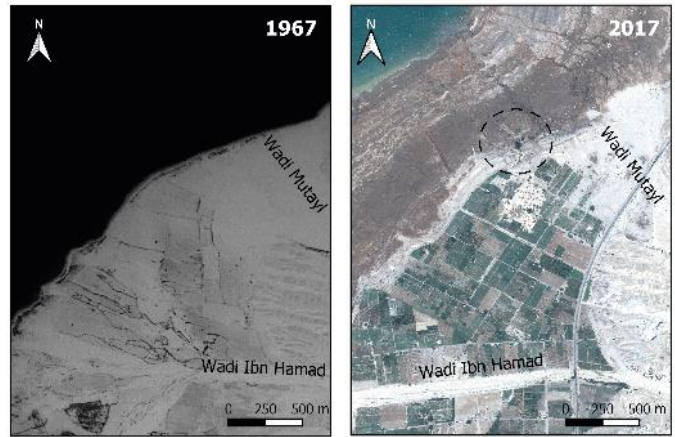


**Table 1: Sources and resolution of remote- and near-sensing data used in this study. RJGC = Royal Jordanian Geographic Centre. The spatial resolution of the dataset varies from 1.8 – 0.1 metres per pixel. The temporal resolution of the dataset is decadal from 1970 – 2010, and annual from 2004 – 2017. On the right are images of the southern part of the study area from 1967 and 2017 demonstrating the evolution of geomorphology and land use change in the study area. Black dashed ellipse marks the site of the former Numeira Mud Factory.**

## 4 Results

### 4.1 Base level fall, shoreline retreat and bathymetry

215 The Dead Sea level drop has resulted in a dramatic retreat of the shoreline in the Ghor Al-Haditha area  
(**Figure 2A**). As of 2017, the shoreline had retreated from its 1967 position by a minimum of 0.3 km in  
the north of the study area and by a maximum of 2.5 km in the south. The rate of retreat in the southern  
part of the study area accelerated from  $< 10 \text{ m yr}^{-1}$  between 1967-1980 to an average rate of  $\sim 45 \text{ m yr}^{-1}$   
220 about 7-8  $\text{m yr}^{-1}$ . The pre-recession bathymetry was steepest in northern part of the study area (**Figure 3**),  
reflecting its proximity to the escarpment of the Eastern Boundary Fault of the Dead Sea basin (**Figure**  
**1A, C**). The southern part of the area had a gentler bathymetry (**Figure 2**), possibly reflecting the  
extensive Plio-Pleistocene and Holocene fan deposition at the terminations of several major wadis  
(**Figure 1B, C**).

225

The rate of shoreline retreat is correlated non-linearly with the former bathymetric slope (**Figure 2D**).  
Following Bruuns' Rule of coastal erosion, a theoretical relationship between slope and the rate of  
shoreline retreat assuming a constant rate of base level drop (Bruun, 1988) is as follows:

$$R_{DS} = \frac{Z_{DS}}{\tan\alpha} \quad (1)$$

230

, where  $R_{DS}$  is the rate of retreat of the Dead Sea shoreline,  $Z_{DS}$  is the average rate of Dead Sea level drop  
for the time period being analysed, and  $\alpha$  is the slope of the former Dead Sea bed. The data are well  
explained by the theoretical retreat rate vs slope curves calculated for cases of base level fall rates of  $0.5$   
 $\text{m yr}^{-1}$  (1960-2000) and  $1.1 \text{ m yr}^{-1}$  (2000-2017). Therefore, the shoreline retreat rates are partly influenced  
by the gradually accelerating rate of base level fall, but they are mainly related to the relief of the former  
235 bathymetry.

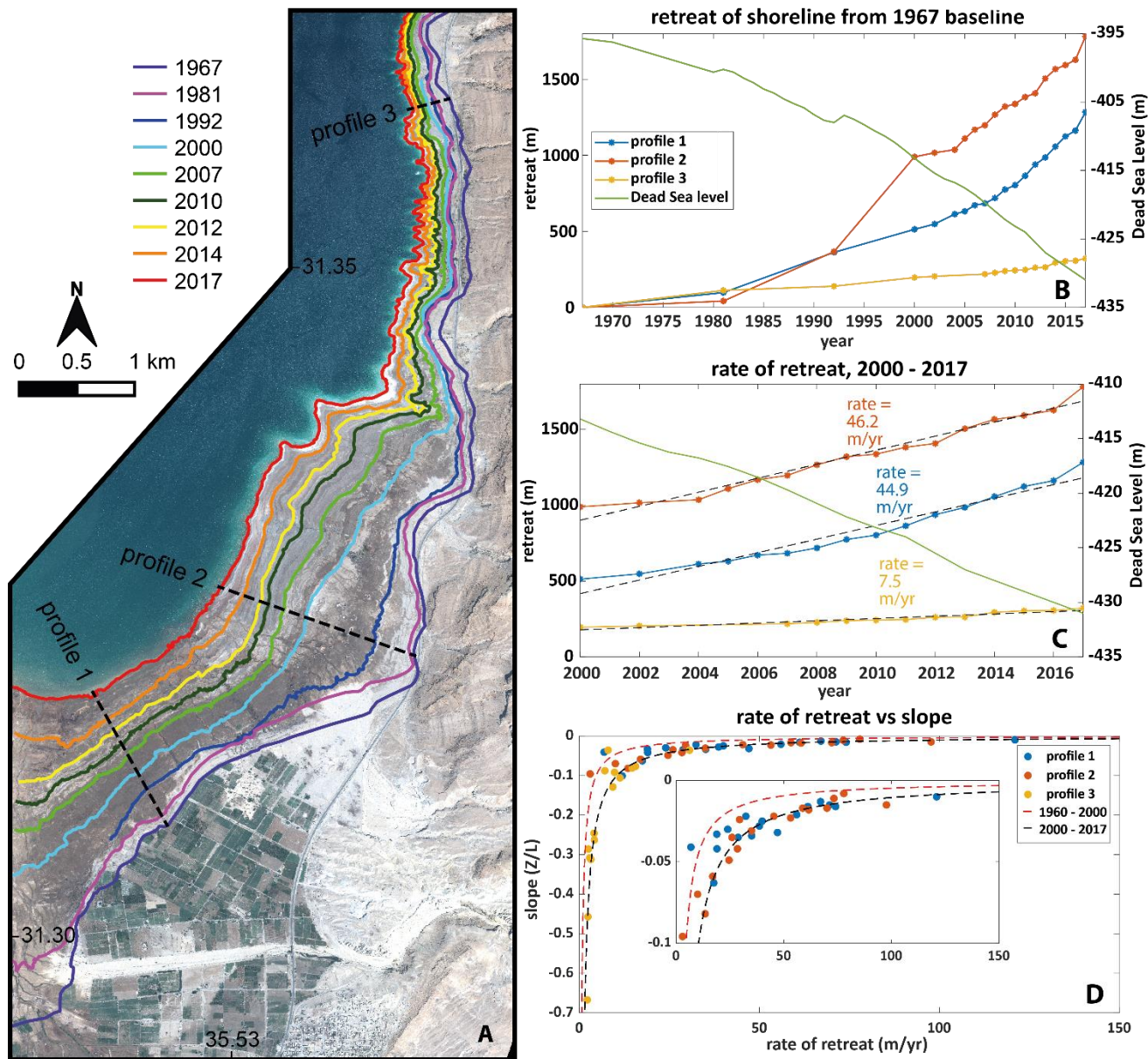


Figure 2: Dead Sea level fall and shoreline retreat in the Ghor Al-Haditha area of Jordan from 1967-2017. (A) Map of shoreline retreat with time, produced from satellite and aerial imagery. Also shown here are plots of the Dead Sea Level and of the shoreline position along profiles in the Ghor Al-Haditha area over the periods: (B) 1967-2017 and (C) 2000-2017. (D) Plot of rate of shoreline retreat against bathymetric slope for Profiles 1-3. The inset shows a close-up of the data from Profiles 1-2 for clarity.

## 4.2 Widespread subsidence of the former lakebed

245 Comparison of the reconstructed lake bathymetry with the 2016 DSM reveal several substantial elevation changes since lake recession (**Figure 3**). The negative differences in elevation **reveals** a pattern of subsidence of 0 – 6m across the former lakebed in the southern part of the study area over distances on the kilometre scale (profiles A and B). This wide-scale subsidence consistently diminishes seaward to the position of the 2017 shoreline, where elevation difference tends to zero across the study area. The south-east end of Profile A also captures more localised subsidence due to development of an uvala-like  
250 depression, of which a number of similar zones of subsidence can be seen across the central part of the study area (for details, see section 4.4). Subsidence of 0 – 3m occurs also in the areas of exposed lakebed in the north of the study area, as outlined by the elevation difference along profile C, although these are on a smaller spatial scale **in keeping** with the smaller shoreline retreat there.

255 Positive elevation changes occur near the 1967 shoreline in the southern and northern parts of the study area. Those in the south coincide with the active alluvial fan at the mouth of the Wadi Mutayl, as well as with areas of vegetation growth (trees and bushes) and/or anthropogenic **activates** (e.g. earthworks at the former Numeria Mud Factory site). Large positive elevation differences in the north coincide with the main north-south highway, which was constructed in the early 1990s.

260

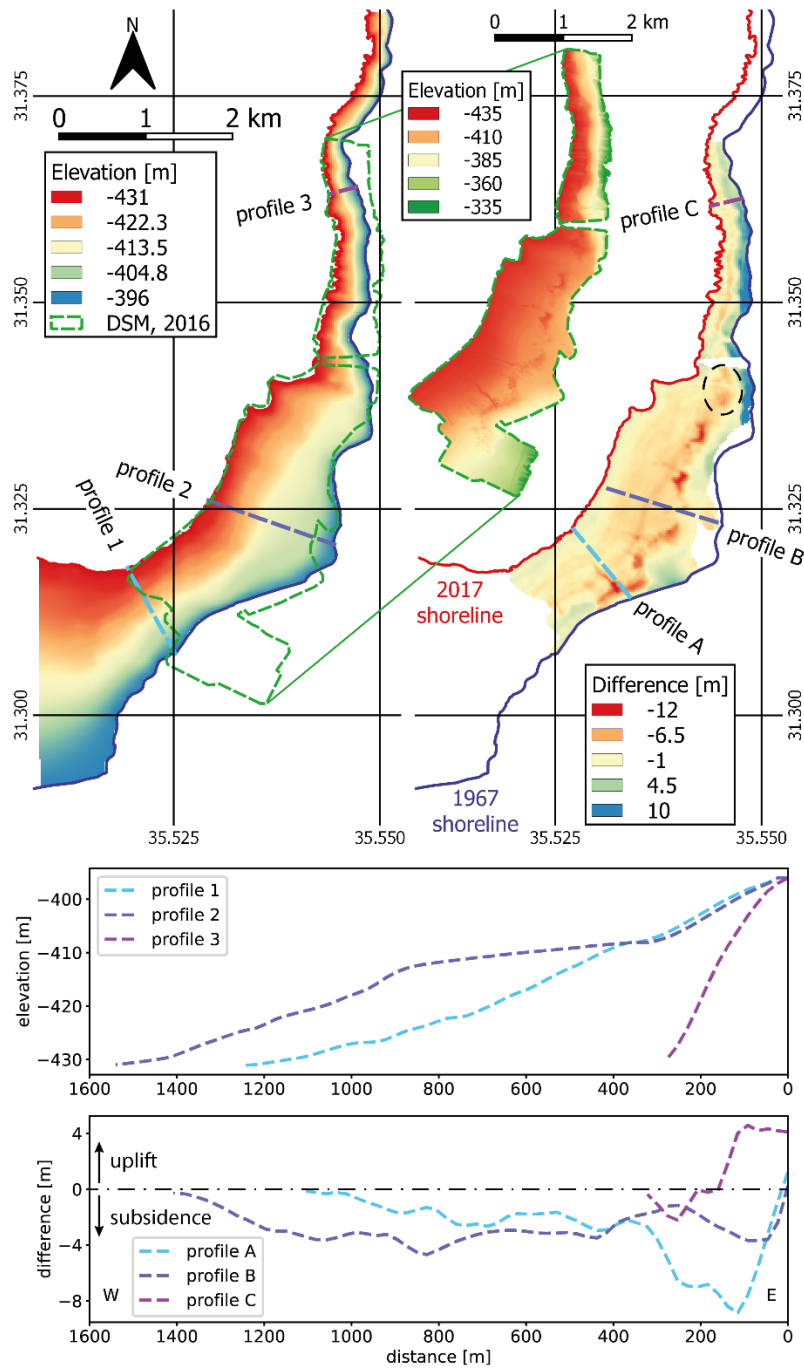


Figure 3: bathymetric contour map of the relief of the former lakebed (top left), with an inset of the 2016 DSM relief and elevation profiles 1-3 (as in Figure 3) plotted second from bottom. Top right: map of elevation difference between the former lakebed bathymetry and the 2016 topography. Areas of high subsidence are identifiable by the large negative difference (see 0 – 300m along profile C, bottom plot). There is subsidence of between 0 – 6m on the kilometre-scale in the southern part of the study area (profiles A and B), with subsidence of 0 – 3m on a smaller scale in the northern part of the study area (profile C). The dashed black ellipse indicates a zone of developing subsidence referred to in section 4.4.

### 4.3 Sinkhole development and morphology

Sinkhole formation began at Ghor Al-Haditha in the mid-1980s in the southern part of the study area (**Figure 4**). Initiation of new sinkhole development subsequently shifted north-northeast-ward, roughly parallel to the coastline. In detail, the sinkholes have initiated in clusters, with gaps between earlier clusters filled or reduced as new sinkholes and new sinkhole clusters form. The most active area is now adjacent the Dead Sea highway in the northern part of the study area.

After initiation in a given sub-area, further new sinkhole development within that sub-area has generally migrated seaward – i.e. westward or north-westward. The extent to which new sinkhole development has migrated seaward varies between 100 – 500 m, but is observed consistently all along the line of the currently mapped sinkhole population. Overall, we estimate that at least ~1150 sinkholes have formed in the area between 1985 and 2017.

The size and morphology of individual sinkholes is linked to the nature of the near-surface deposits in which they form (**Figure 5**). Depending on the dominant material surrounding each sinkhole at the surface, as visible from orthophotos and field observations, we assigned sinkholes into three groups: alluvium, lacustrine ‘mud’ and lacustrine ‘salt’ (the latter comprising also other evaporitic minerals). In general, sinkhole diameter ranges from 1 - 70 m (**Figure 5A**). The distribution of diameters is skewed toward lower values, however, such that the mode of sinkhole diameter is 4 – 8 m in ‘salt’, 4 – 12 m in alluvial sediments, and 8 – 16 m in lacustrine ‘mud’. The skew is most pronounced for sinkholes in the lacustrine ‘mud’, the diameter of some of which is over 70 m.

The depth/diameter ratios of sinkholes in lacustrine ‘mud’ and ‘salt’ are lower (average  $De/Di = 0.18 \pm 0.09$  and  $0.16 \pm 0.08$  respectively) than the sinkholes in ‘alluvium’ (average  $De/Di = 0.38 \pm 0.17$ ) (**Figure 5B**). For linear regression models calculated for depth against diameter, sinkholes in alluvium show the least variance; sinkholes in mud show the most variance. Regardless of the surface materials in which they occur, eccentricity of sinkhole circumferences is usually 1 – 2; values greater than 2 are rare (**Figure**

300 **5C).** The azimuths of the long axes of all sinkholes show a general E – W alignment (**Figure 5D**), which is broadly parallel to the average aspect of the slope for the study area.

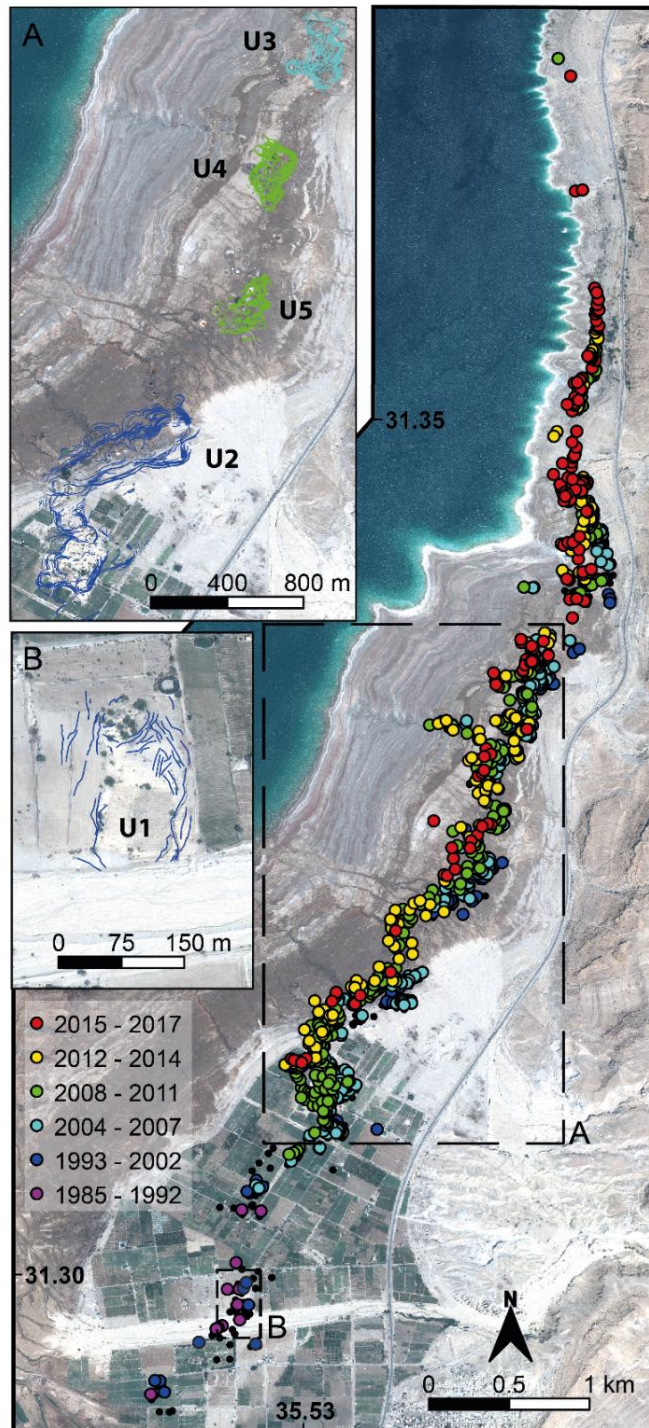


Figure 4 (page 15): Sinkholes mapped from satellite and aerial imagery, colour-coded by year of first sighting in time intervals as labelled. Base image is Pleiades 2017. Smaller black dots are sinkholes mapped prior to 2009 by other sources but not visible in our imagery. Insets A and B show the larger-scale depressions, as denoted by mapped ground cracks and fractures. For clarity, all fractures for each depression are colour-coded by year of first sighting of any fractures related to that depression. In detail, the fracture formation ages in each large-scale depression span a greater range than shown here (see Figures 6 and 7).

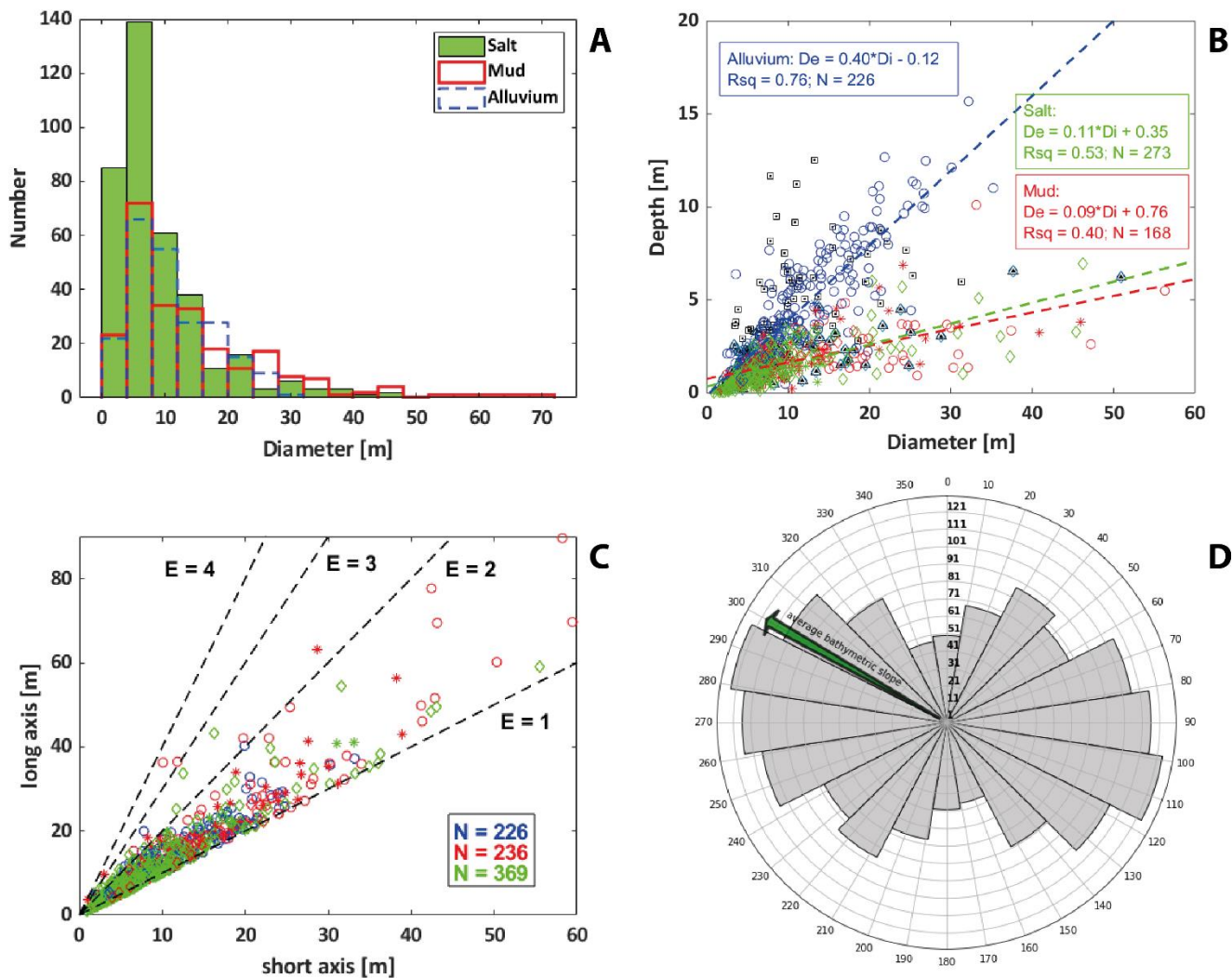


Figure 5: Morphological characteristics of the sinkhole population developed at Ghor al-Haditha in various sedimentary materials. (A) Number of holes binned according to average diameter, (B) the relationship between depth and diameter, and (C) plan-view eccentricity (longest/shortest diameter). (D) rose diagram of azimuth of the long axes of all sinkholes in the study area, with the average aspect of bathymetric slope plotted for comparison (green arrow). Each concentric circle represents a count of 10 sinkholes. The total number of holes analysed is 226 in the alluvium, 236 in the mud-dominated lacustrine deposits ('mud') and 369 in the salt-dominated deposits ('salt'). Water-filled holes were excluded from the depth/diameter analysis. The De/Di plot presents the maximum elevation difference between the rim and the bottom of each sinkhole. Black squares in (B) are De/Di for sinkholes formed in alluvium derived from Filin et al. (2011); the black triangles are De/Di for sinkholes formed in mudflats also derived from Filin et al. (2011).



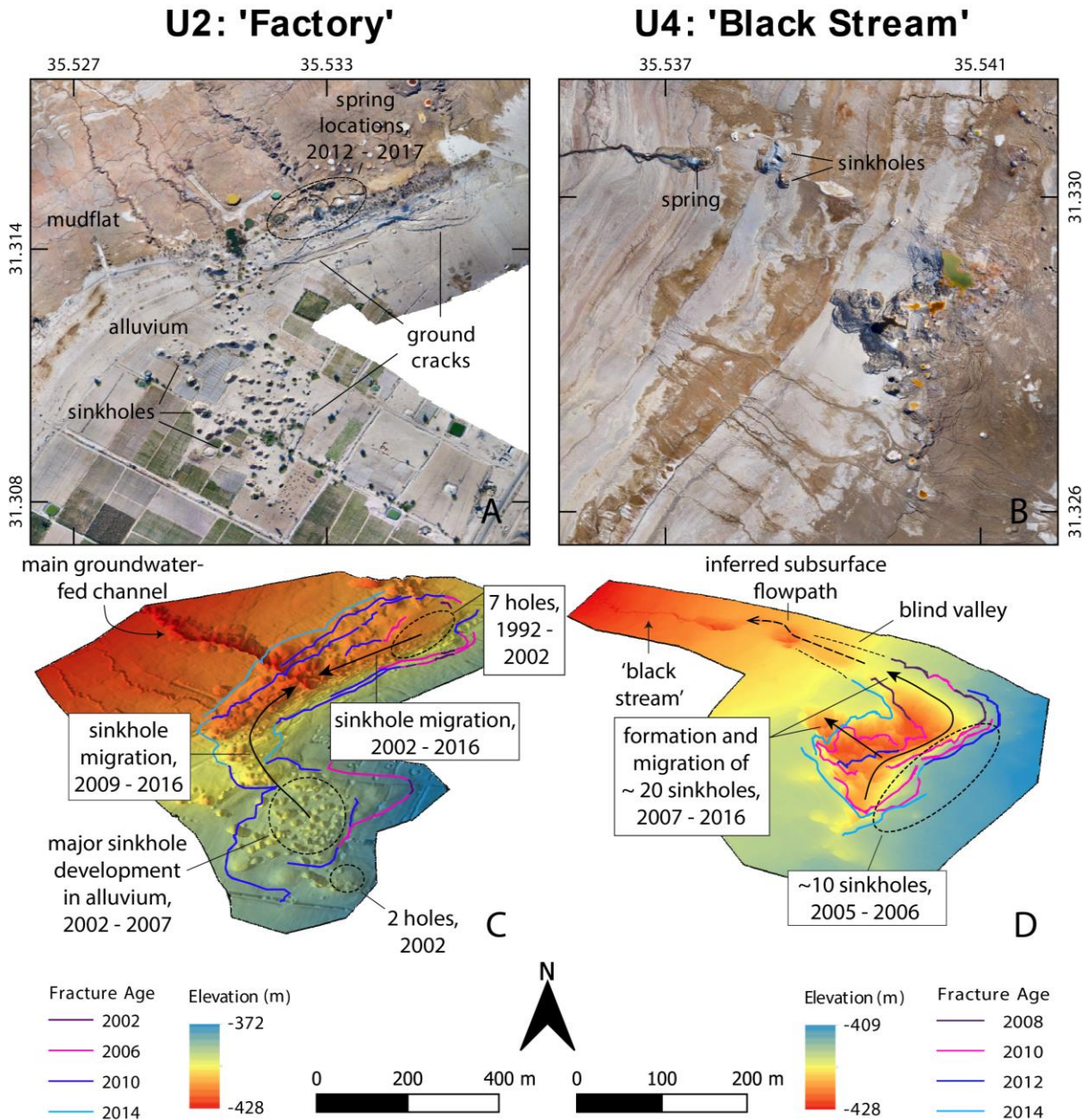
#### 4.4 Uvala development and morphology

320 The uvalas in the study area are gentle depressions of several hundred metres in lateral extent of non-uniform shape that enclose numerous sinkholes (**Figures 4, 6 & 7**). These uvalas have  $D_e/D_i$  ratios of 0.016 – 0.042, calculated using the method suggested by Čalić (2011) of considering the diameter of a circle of equivalent area and taking the maximum depth. The uvalas are bounded partly by systems of ground cracks and/or faults. The ground cracks are dominantly opening mode fractures with apertures of up to 30 cm, while the faults are shear fractures with vertical displacements of the ground surface up to 325 1.5 m. Mixed opening- and shear-mode fractures are also observed. The expression of such fractures is material-dependent. In alluvium, subsidence-related displacements are accommodated on fewer but larger fractures, whereas in mud-rich lacustrine deposits such displacements are accommodated on more numerous but smaller fractures. As shown below, these fracture systems are spatially and temporally associated with subsidence of each uvala. They are not to be confused with regional tectonic structures.

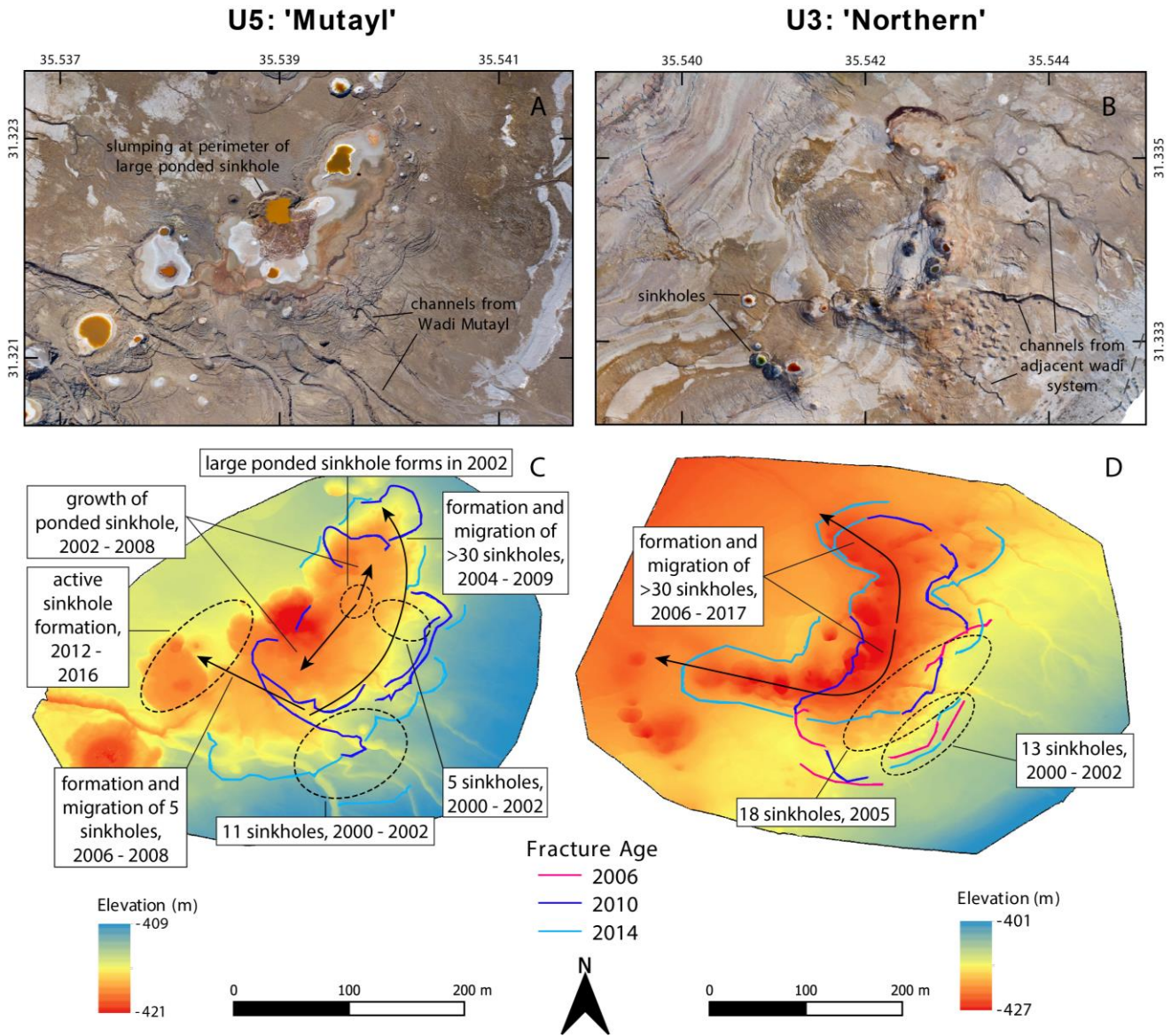
330 Development of each uvala appears to follow precursory sinkhole formation at that site (prior to the first remotely sensed ground cracking associated with the uvala). About 2 – 8 years after the first sinkhole sighting (in which time many new sinkholes have generally clustered about the initial holes), ground cracks develop that no longer trend concentrically to any single sinkhole, but instead delineate a wider zone of subsidence that envelopes several sinkholes or even several clusters of sinkholes. The first uvala, 335 U1, developed between 1992 and 1999 in the south of the area, near the Wadi Ibn Hamad (**Figure 4**). U2 and U3 initiated in 2002 and 2005-2006, respectively, to the north east of U1. Both U4 and U5 began forming around 2008, but lie between U2 and U3. Additionally, a wide area of m-scale subsidence detected in the bathymetry-topography DEM differencing (black dashed ellipse, **Figure 3**), along with 340 some initial ground cracking patterns observed in the 2015 and 2016 orthophotos in that area, suggest that a new uvala U6 is developing further northeast of U3. In general therefore, younger uvalas have formed to the northeast, as seen for the sinkholes, although not (yet) in as clear a sequence.

345 After initiation, uvala growth is closely linked with further sinkhole formation within it. For instance, groundcracks related to U2 initiated around two spatially-discrete sinkhole clusters; these fractures sets

propagated and joined as sinkhole development migrated seaward (**Figure 6**). For both U3 and U4, two ‘prongs’ of coevally-migrating ground **crack** and sinkhole development are visible (**Figures 6 and 7**). Again, the direction of uvala growth has generally been seaward. The end of uvala growth is also linked with the end of sinkhole development; this is exemplified by uvala U1, which ceased development by 2006, in tandem with cessation of sinkhole activity nearby.



355 **Figure 6 (page 18): Structural development of uvalas with demonstrable connection to channelized subsurface water flow. See figure 5 for locations. (A) and (B) show orthophoto images from 2016; (C) and (D) show oblique 3D views of the depressions derived from the 2016 DSM. The main depression-bounding fractures are shown, whose years of formation (i.e. when first visible in imagery) are grouped and coloured in four-year intervals for U2 and in two-year intervals for U4. Each uvala is linked morphologically to a highly active stream that emerges on the seaward side at several meters below the surrounding ground surface.**



360 **Figure 7: Structural development of uvalas U5 and U3 with unclear connection to subsurface water flow. See figure 5 for locations. (A) and (B) show orthophoto images from 2016; (C) and (D) show oblique 3D views of the depressions derived from the 2016 DSM. The main depression-bounding fractures are shown, whose years of formation (i.e. when first visible in imagery) are coloured in four-year intervals.**

365

#### 4.5 Links between subsurface stream flow and the formation of sinkholes and uvalas

Several features of the uvalas and the formation of sinkholes within them strongly suggest a link between their development and the channelized flow of relatively fresh groundwater in the subsurface. The best example of such links is seen **at** uvala U2, close to the former Numeira Mud Factory site. The history of this uvala occurs in close association with the development of the system of stream channels which drain the superficial aquifer within the deposits of the Wadi Ibn Hamad. This stream channel system has **localised** from several small channels **to** one ‘main channel’ over time. This main channel formed late in the system evolution and, unusually, it developed by rapid retrogressive (upslope, headward) erosion (Al-Halbouni et al., 2017). This new channel developed from a spring, the exact location of which has changed several times since its inception, which emerged in the middle of the saline mudflats and in association with drainage of a lake hosted in U2 (**Figure 6**; c.f. Fig. 16, Al-Halbouni et al., 2017). The migration patterns of sinkholes within U2 over time converge at the spring location, as the two initially separate zones of subsidence coalesce as shown (**Figure 6**). Upstream incision at the head of the channel is spatially and temporally linked with sinkhole collapses, which occurred on a time-scale of a few days. These collapses suggest that the water flowing in the channel reaches its head via subsurface conduits, which are the cause of subsurface instability related to the surface collapse and sinkhole formation.

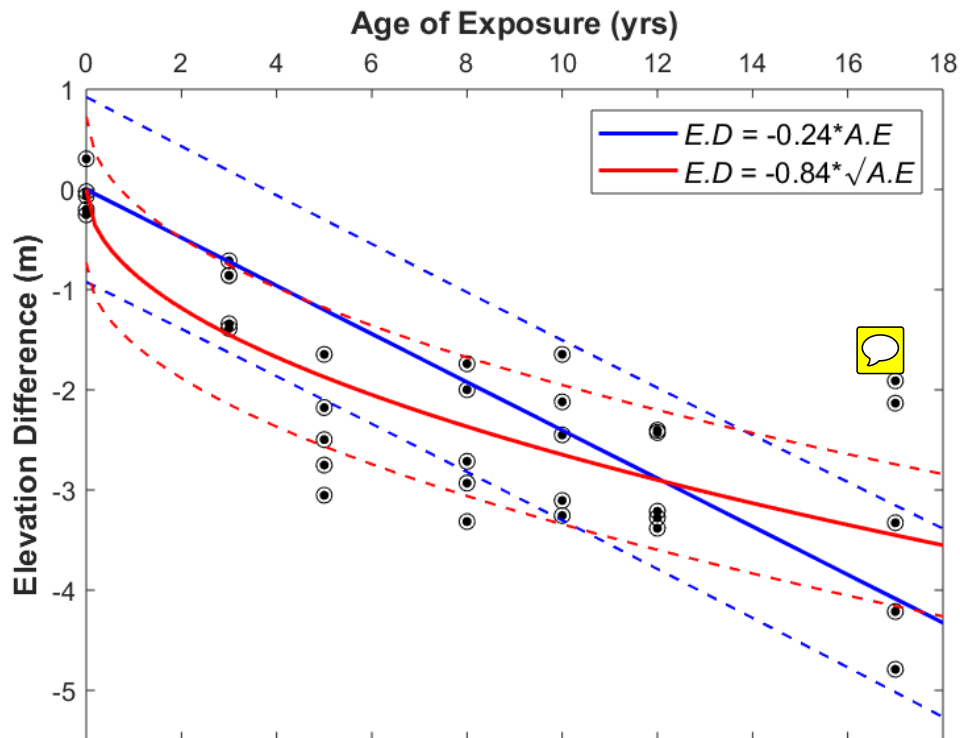
Further evidence of such links is seen at Uvala U4, which is linked spatially and temporally with another artesian spring which feeds a similar meandering stream channel (**Figure 6**), that we have termed the ‘black stream’ (due to the very dark-coloured water that flows within it). Initial ground cracking at U4 occurred proximal to a subtle linear depression (or ‘blind valley’) between it and the spring feeding the ‘black stream’, which we first observe in satellite images from 2009. The migration of sinkholes within U4 seems to follow a flow path from the initial pre-uvala sinkhole cluster to the ‘black stream’ head, suggesting the presence of a flow conduit beneath the depression. The additional ‘prongs’ of sinkhole migration and ground cracking at uvalas U4 and U3 (**Figures 6 and 7**) may also represent a surface expression of subsurface conduit development, although no associated springs have yet been observed.

## 5 Discussion

Our reconstruction of the former Dead Sea bathymetry in the Ghor Al-Haditha study area combined with the DSMs from our photogrammetric surveys has revealed subsidence on three area scales: (1) a  $\sim 3 \times 10^6$  m<sup>2</sup> sized swath of distributed subsidence affecting the lacustrine deposits of the former Dead Sea bed; (2) several  $3 \times 10^4 - 5 \times 10^5$  m<sup>2</sup> sized zones of more localised subsidence (uvalas); and (3) numerous  $1 \times 10^0 - 7 \times 10^1$  m<sup>2</sup> sized features of highly localised subsidence (sinkholes). In this section, we focus our discussion first on the former of these phenomena; the latter two are discussed in detail subsequently.

### 5.1 Distributed subsidence of the former Dead Sea bed following base level fall

The distributed subsidence of the former lakebed increases systematically in magnitude from zero at the 2017 shore line to a maximum of about 4 or 5 m near the shoreward edge of the lacustrine deposits. The magnitude of subsidence in the lakebed area lying between the 2000 - 2017 shorelines correlates with the age of emergence of the lakebed as the Dead Sea has receded (**Figure 8**). Data from the predominantly alluvial area lying between the 1967-2000 shorelines and from the northern-most part of the study area are excluded from this figure, because these are demonstrably subject to confounding influences from alluvial erosion/deposition, karstification and, most significantly, anthropogenic landscape disturbance (infrastructural development). The data in **Figure 8** are fit well by a function in which subsidence magnitude varies linearly with time, and they are fit slightly better by a function in which subsidence magnitude varies a function of the square root of time. In agreement with Baer et al. (2002), we regard the most likely driving mechanism for the observed distributed subsidence of the former lakebed to be consolidation and compaction of the formerly water-logged evaporite and marl deposits upon the lowering of the Dead Sea level.



415 **Figure 8:** Plot of lakebed subsidence against time since exposure. The elevation difference is modelled as varying linearly (thick blue line) and non-linearly (thick red line) with the age of exposure of the lakebed. Dashed blue and red lines represent the 95% confidence limits. Elevation difference is measured between the reconstructed bathymetric DSM and the 2016 topographic DSM at the intersection points of the several profiles taken parallel with the direction of shoreline retreat as they transect the 2017, 2014, 2012, 2009, 2007, 2005 and 2000 shorelines. Age of exposure is with respect to 2017.

420 A non-linear subsidence rate model, as shown in **Figure 8**, is more compatible than a linear model with the distribution and magnitude of subsidence rates of the lakebed as reported previously from InSAR analysis (Baer et al., 2002; Fiaschi et al., 2017; Nof et al., 2019; [Yechieli et al., 2015](#)) and from differencing of LiDAR-derived DSMs (Avni et al., 2016). In general, the rate of subsidence of the former lakebed in these reports decreases landward from the contemporary shore line. The magnitude of

425 subsidence rates previously reported are up to 0.18 - 0.30 m/yr immediately adjacent **the** contemporary shore line, with magnitudes of 0.01 – 0.15 m/yr further landward. The non-linear rate of subsidence modelled in **Figure 8** would give a rather high initial subsidence rate of 0.53-0.65 m/yr in the first two years after emergence, but this rate would decline to 0.10-0.13 m/yr in the 10-17 years after emergence. The latter rate agrees well with InSAR-derived subsidence rates of 0.05 – 0.15 m/yr adjacent to the 2000

430 shoreline around Ghor Al-Haditha and the Lisan peninsula (Fiaschi et al., 2017). Our results thus represent

the first ground validation of InSAR-based detection of distributed subsidence of the former lakebed at the Ghor Al-Haditha study site.

## 5.2 Morphological attributes of sinkhole and uvalas in evaporite karst

435 The sinkholes and uvalas in the evaporite karst setting of the Dead Sea are distinct in terms of their scale and morphology. The uvalas are much more irregular in plan-view than the sinkholes, and they enclose numerous sinkholes, including coalesced sinkholes and clusters of sinkholes. The uvalas also have depth/diameter ratios ( $De/Di = 0.016 - 0.042$ ) up to two orders of magnitude lower than the sinkholes ( $De/Di = 0.02 - 1.80$ ).

440 These morphological characteristics of the evaporite karst sinkholes and uvalas are similar to those in some limestone karst settings. In data from the limestone karst of Trieste as reported by Bondesan et al. (1992), for example, diameters of sinkholes (dolines) show a positively-skewed distribution and a range of depth/diameter ratios ( $De/Di = 0.04-0.40$ ) similar to those observed for the evaporite karst sinkholes at Ghor Al-Haditha. Moreover, the range of depth/diameter ratios of uvalas in the Dinaric and Carpatho–Balkanides limestone karst ( $De/Di = 0.016-0.10$ , as reported by Čalić (2011)) overlaps that of the  
445 evaporite karst uvalas. In both limestone and evaporite karst examples, the uvalas are far greater in size, have a more irregular form and have far lower depth/diameter ratios than the sinkholes (dolines). The main difference between the respective depression types of each karst setting is the absolute size. Sinkholes and uvalas in the evaporite karst of the Dead Sea are considerably smaller than their equivalents in the limestone karst, possibly as a result of the greater material strength and potential depth of  
450 karstification in the limestone regions (Al-Halbouni et al., 2018, 2019; Čalić, 2011).

The relationship between surface materials and sinkhole morphology in the Dead Sea evaporite karst setting is well known (Filin et al., 2011; Al-Halbouni et al., 2017). The low vs high  $De/Di$  ratios of the sinkholes in ‘mud’ and ‘alluvium’, respectively, have been attributed previously to a contrast in the  
455 strength (Al-Halbouni et al., 2018, 2019) and/or rheology (Shalev and Lyakhovsky, 2012) of these materials. Expanding upon data presented in these previous works, we show that  $De/Di$  ratios of sinkholes formed in ‘salt’ generally fall between those of sinkholes formed in ‘alluvium’ or ‘mud’ (Figure 5B).

This probably reflects the observation that near-surface deposits dominated by ‘salt’ layers usually contain a considerable proportion of ‘mud’ layers, and so the mechanical behaviour of ‘salt’ is weakened. Compared to those in mud-rich sediments or alluvium, sinkholes formed in the salt-rich sediments also have generally smaller diameters (**Figure 5A**). This could reflect a scaling limit imposed by the level of karstification, which field evidence locally shows is at, or within a few metres of, the surface in the salt-rich material in the northern part of the area. The effect of material property on the uvalas is seen mainly in the expression of the marginal fracturing, which as for sinkholes, is more sharply defined in the higher strength alluvium (see also Al-Halbouni et al., 2018). However, the data are too few to determine any material-linked differences in depth/diameter ratio of the uvalas.

### **5.3 The formation of uvalas and their inter-relationship with sinkholes**

The processes governing the genesis of uvalas are debated in karst geomorphology (Ćalić, 2011; Kranjc, 2013; **Lowe and Waltham, 1995**). As summarised by Ćalić (2011), three main end-member mechanisms for the formation of uvalas in limestone karst have been proposed: (1) large-scale lowering of the landscape by dissolution of material at the surface and in the vadose zone; (2) areally-distributed sub-surface mass-wasting (corrosion) of soluble material, possibly enhanced along tectonic fractures; (3) coalescence of sinkholes. Here we discuss the relevance of these three end-member mechanisms for the genesis of the uvalas related to evaporite karstification in our study area.

Surface dissolution and sinkhole coalescence can be precluded as major mechanisms for uvala formation in the evaporite karst setting of Ghor al-Haditha. Much of the surface material affected by uvala formation is non-karstic (non-soluble alluvium), and the hyper-arid climate conditions of the study area probably limit any solution in the vadose zone. Although sinkhole coalescence occurs at Ghor al-Haditha, resulting in compound sinkholes both within and outside of an uvala, this process is not responsible for the main morphometric attributes of the uvalas. The uvalas are observed to develop as larger-scale depressions that have distinct morphometric attributes and limits, both in space and time (**Figures 4, 6 and 7**).



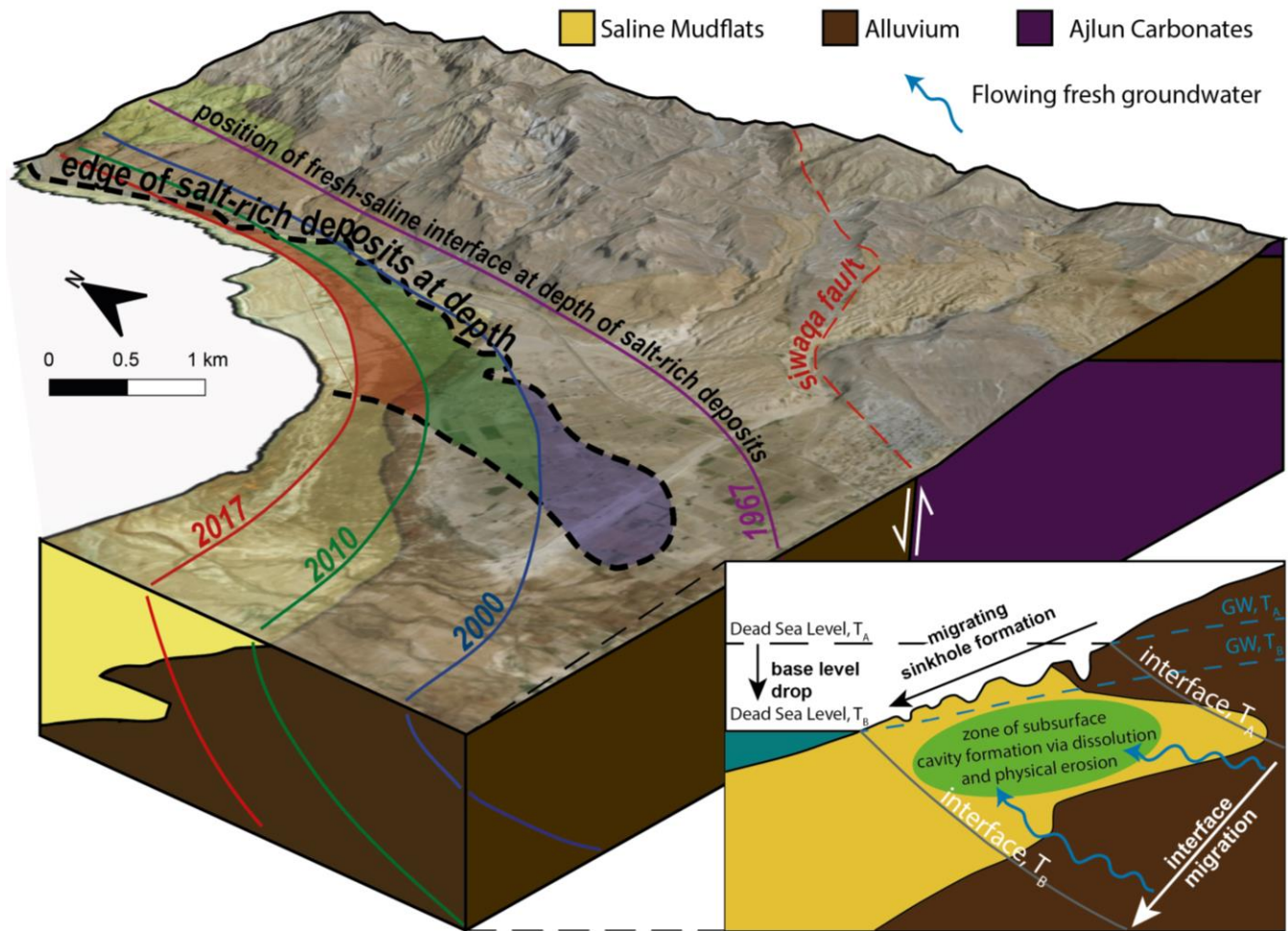
Our observations are consistent with a mechanism of uvala formation by areally-distributed sub-surface  
485 corrosion and erosion, which results in a broad lowering of the surface by subsidence. Our observations  
further show that an uvala initiates, evolves and ceases in tandem with sinkhole development within it.  
These observations are broadly consistent with modelling of subsidence produced by the development of  
multiple void spaces at progressively deepening levels with varying individual growth rates (Al-Halbouni  
et al., 2019). We propose that this indicates the same overall formation process for both types of enclosed  
490 depression, but that the morphological expression of the process differs depending on the scale at which  
the process operates. Uvalas can be considered ~~to be~~ the integrated subsidence response of dissolution  
and mechanical erosion distributed over a mechanically unstable subsurface volume (e.g. a groundwater  
conduit network). Sinkholes, on the other hand, represent discrete subsidence responses within that volume  
to smaller-scale zones of highly localised material removal and related instability (e.g. in an individual  
495 groundwater conduit).

It is beyond the scope of the current study to resolve general relevance of the subsidence mechanism of  
uvala formation in evaporite karst for areas of limestone or gypsum karst. One must of course be conscious  
that similarity of form does not necessarily mean similarity of genesis. Future work might involve  
500 resurveying uvalas in limestone karst areas for structural evidence of uvala-scale subsidence, such as  
synclinal bed rotations and marginal fractures (fissures and/or faults) that are geometrically and  
kinematically linked to the uvala. Although sparse, structural data presented for the Grda Draga uvala in  
the limestone Dinaric karst, Slovenia (Fig. 4 of (Ćalić, 2011)) seem broadly consistent with a genesis  
through subsidence. In limestone karst areas, regional tectonics may facilitate (and complicate) uvala  
505 formation by, for instance, providing zones of enhanced permeability for groundwater flow (Ćalić, 2011).  
Additionally, in limestone karst, most uvalas do not have water at their bottoms (Calic 2011), whereas  
water has occupied (ephemerally or otherwise) the bottom of some of our evaporite karst uvalas. Hence  
the relationship of uvalas to the water table may vary from one karst environment to the other, in line with  
the dissolution dynamics of each. Future studies with more detailed datasets are required to test whether  
510 the mechanisms of uvala development in evaporite karst in our study area are applicable to limestone and  
gypsum karst areas.

#### 5.4 Effects of base-level fall on the spatio-temporal pattern of sinkhole and uvala development

At the kilometre scale, the spatial distribution of sinkholes and uvalas at Ghor Al-Haditha follows two linear trends: a N24° trend in the south and a N0° in the north (**Figure 4**). These trends match those of main regional faults in the Dead Sea transform (**Figure 1A, C**) and so indicate some tectonic control (cf. 515 Abelson et al., 2003; Closson, 2005; Yechieli et al., 2015), the nature of which has been debated. Some authors have envisaged that tectonic faults conduct ground water directly into evaporite deposits (**Charrach, 2018; Closson and Abou Karaki, 2013**), while others suggest that tectonic faults control the initial depositional geometry of evaporite deposits (**Ezersky et al., 2013; Frumkin et al., 2011; Frumkin 520 and Raz, 2001**). In closer detail (hundred-metre scale), the sinkhole distribution at Ghor Al-Haditha is rather non-linear (**Figure 4**). This non-linearity may reflect control from the distribution of salt-rich evaporite deposits at depth (Ezersky et al., 2013), and thus reflect the palaeo-shoreline, as determined by the regional fault systems on the larger scale.

525 The spatio-temporal development of sinkholes and uvalas at Ghor Al-Haditha shows two striking features. Firstly, new sinkholes and uvalas **has** successively formed along a SSW→ NNE trend with time, i.e. roughly shoreline parallel (**Figure 4**). Secondly, after they have been established in a given part of the study area, the formation of new sinkholes and the growth of the uvalas occurs consistently **seaward** direction, i.e. roughly shoreline perpendicular (**Figures 4, 6 & 7**). Both of these observations are 530 qualitatively consistent with the predicted migration of this dissolution front in the response of sinkhole population evolution to base level fall, especially if the migration of the fresh/saline interface is considered to intersect obliquely with the distribution of salt-rich evaporite deposits in the subsurface (**Figure 9**). Although constraints on the fresh-saline interface from boreholes or geophysical techniques are lacking in the Ghor Al-Haditha study area, the systematic spatio-temporal migration of new depression 535 development **provide** strong evidence that a seaward shift of the fresh-saline interface induced by base-level fall is a key control on sinkhole development here. A future definitive analysis of the sinkhole and uvala migration should include a borehole drilling campaign in the study area, similar to that conducted on the western shore (**Abelson et al., 2017; Yechieli, 2000**).



540 Figure 9: hypothetical interaction of a migrating fresh-saline interface with sub-surface salt-rich deposits. The shaded coloured areas depict the expected zones of sinkhole development for different time periods as a result of convergence between the salt-rich deposits at depth and the fresh-saline interface: blue = 1985 – 2000; green = 2000 – 2010; red = 2010 – 2017. ‘Salt-rich deposits’ here refers to deposits rich in numerous different evaporites. The inset shows the conceptual model of seaward migration of sinkhole populations at the Dead Sea as the fresh-saline interface migrates with the base level drop, as outlined in section 1, after Abelson et al. (2003, 2017), Yechieli (2000) and Salameh and El-Naser (2000). ‘GW’ here refers to the inferred level of the groundwater in the subsurface.

545

## 6 Summary & Conclusions

Our results provide, for the first time, a detailed picture of the interlinked geomorphological development of sinkholes and uvalas in an evaporite karst setting. They also provide new insights into **to** impact of base level fall on **that** development **at** the Dead **Sea**. Based on the combination of remote sensing data, photogrammetric surveying and field observations, our main findings with respect to the Ghor Al-Haditha study area on the eastern shore of the Dead Sea are as follows:

550

- 555 (1) At least 1,100 collapse sinkholes and five uvalas have formed by subsidence in the evaporite karst setting of Ghor Al-Haditha since the mid-1980s. The developments of individual uvalas and of sinkhole populations within them are intertwined in terms of onset, evolution and cessation. While many sinkholes develop initially in clusters, the uvalas develop as a larger-scale, gentler and structurally-distinct depressions around such clusters.
- 560 (2) The studied evaporite-karst uvalas likely form through subsidence in response to distributed subsurface dissolution and erosion within a mechanically unstable subsurface volume (e.g. a groundwater conduit network). Sinkholes, on the other hand, represent discrete subsidence responses within that volume to smaller-scale zones of highly localised material removal (e.g. in individual groundwater conduits) and related instability. In agreement with inferences for examples in limestone karst settings, the uvalas in the studied evaporate karst setting do not form by coalescence of sinkholes. Surface dissolution as a mechanism for uvala formation is not significant in this hyper-arid setting.
- 565 (3) The exposed former Dead Sea lakebed at Ghor Haditha has also undergone a wider-scale subsidence of up to several metres that decreases toward the present-day shore line. Subsidence rates estimated here by DSM differencing are in line with those estimated previously by remote sensing. This wider-scale subsidence is possibly related to post-recession compaction/consolidation of the near surface lakebed sediments upon withdrawal of pore-fluids as the lake level has fallen.
- 570 (4) The location of new sinkholes and uvalas migrates markedly with time, roughly parallel to the shoreline. After initiated, sinkhole clusters and uvalas also show a marked seaward growth with time. These migration patterns of new depression development are broadly consistent with theoretical predictions of a spatio-temporal control on karstification from a laterally-migrating interface between saturated/under-saturated groundwater, as induced by the base-level fall.
- 575

## 7 Data Availability

A full set of metadata is available upon request. Satellite images: some open access (Corona), but mostly commercial. Aerial images: available at discretion of RJGC. Photogrammetric surveys: raw images, DSMs and orthophotos available upon consultation with the authors. Geological Map 1:50,000 Ar Rabba: available at discretion of MEMR.

## 8 Author Contribution


RAW and EPH led the production of figures and writing of the manuscript. RAW undertook the majority of the data analysis associated with the satellite imagery time series and with the 2015 and 2016 DSMs. Additional satellite imagery processing and data analysis was performed by LS, DAH and EPH. DAH and LS generated the orthophotos and DSMs of the study area using SfM photogrammetry. EPH, DAH, LS, HAR, and AS undertook the field studies and close-range photogrammetric surveys in 2014 – 2016. All authors reviewed and commented on the manuscript, and they contributed to discussions of the data.

## 9 Competing interests

The authors declare that they have no conflict of interest.

## 10 Special issue statement (will be included by Copernicus)

## 11 Acknowledgements

We acknowledge MEMR colleagues for support in fieldwork and other logistical support. The comments of two anonymous reviewers have greatly improved the quality of the manuscript. Part of the work of NAK was done during a sabbatical year supported by the Deanship of scientific research – The University of Jordan. The authors acknowledge financial support from GFZ  the Helmholtz Association's recent Dead Sea Research Venue (DESERVE) initiative (Kottmeier et al., 2016), especially for the associated data and fieldwork costs. Funding for RAW's masters research project, supervised by EPH, was provided by the Geological Survey Ireland under a GSI Short Call grant to EPH (Contract Number: 2017-sc-002).

## 12 References

- Abelson, M., Baer, G., Shtivelman, V., Wachs, D., Raz, E., Crouvi, O., Kurzon, I. and Yechieli, Y.: Collapse-sinkholes and radar interferometry reveal neotectonics concealed within the Dead Sea basin, *Geophys. Res. Lett.*, 30(10), 2–5, doi:10.1029/2003GL017103, 2003.
- 605 Abelson, M., Yechieli, Y., Baer, G., Lapid, G., Behar, N., Calvo, R. and Rosensaft, M.: Natural versus human control on subsurface salt dissolution and development of thousands of sinkholes along the Dead Sea coast, *J. Geophys. Res. Earth Surf.*, 122(6), 1262–1277, doi:10.1002/2017JF004219, 2017.
- Abou-Karaki, N., Fiaschi, S. and Closson, D.: Sustainable development and anthropogenic induced geomorphic hazards in subsiding areas, *Earth Surf. Process. Landforms*, 2295(October), 2282–2295, doi:10.1002/esp.4047, 2016.
- 610 Al-Halbouni, D., Holohan, E. P., Saberi, L., Alrshdan, H., Sawarieh, A., Closson, D., Walter, T. R. and Dahm, T.: Sinkholes, subsidence and subsrosion on the eastern shore of the Dead Sea as revealed by a close-range photogrammetric survey, *Geomorphology*, 285, 305–324, doi:10.1016/J.GEOMORPH.2017.02.006, 2017.
- 615 Al-Halbouni, D., Holohan, E. P., Taheri, A., Schöpfer, M. P. J., Emam, S. and Dahm, T.: Geomechanical modelling of sinkhole development using distinct elements: model verification for a single void space and application to the Dead Sea area, *Solid Earth*, 9(6), 1341–1373, doi:10.5194/se-9-1341-2018, 2018.
- Al-Halbouni, D., Holohan, E. P., Taheri, A., Watson, R. A., Polom, U., Schöpfer, M. P. J., Emam, S. and Dahm, T.: Distinct Element geomechanical modelling of the formation of sinkhole cluster within large-scale karstic depressions, *Solid Earth Discuss.*, in review, 1–30, doi:10.5194/se-2019-20, 2019.
- 620 Asmar, B. N. and Ergenzinger, P.: Long-term prediction of the water level and salinity in the Dead Sea, *Hydrol. Process.*, 16(14), 2819–2831, doi:10.1002/hyp.1073, 2002.
- Avni, Y., Lensky, N., Dente, E., Shviro, M., Arav, R., Gavrieli, I., Yechieli, Y., Abelson, M., Lutzky, H., Filin, S., Haviv, I. and Baer, G.: Self-accelerated development of salt karst during flash floods along the Dead Sea Coast, Israel, *J. Geophys. Res. Earth Surf.*, 121, 17–38, doi:10.1002/2015JF003738. Received, 2016.
- 625 Baer, G., Schattner, U., Wachs, D., Sandwell, D., Wdowinski, S. and Frydman, S.: The lowest place on Earth is subsiding—An InSAR (interferometric synthetic aperture radar) perspective, *Geol. Soc. Am.*

Bull., 114(1), 12–23, doi:10.1130/0016-7606(2002)114<0012:TLPOEI>2.0.CO;2, 2002.

630 **Bartov**, Y., Stein, M., Enzel, Y., Agnon, A. and Reches, Z.: Lake Levels and Sequence Stratigraphy of Lake Lisan, the Late Pleistocene Precursor of the Dead Sea, *Quat. Res.*, 57(01), 9–21, doi:10.1006/qres.2001.2284, 2002.

**Bondesan**, A., Meneghel, M. and Sauro, U.: Morphometric analysis of dolines, *Int. J. Speleol.*, 21(1/4), 1–55, doi:10.5038/1827-806x.21.1.1, 1992.

635 **Ten Brink**, U. S. and Flores, C. H.: Geometry and subsidence history of the Dead Sea basin: A case for fluid-induced mid-crustal shear zone?, *J. Geophys. Res.*, 117, doi:10.1029/2011JB008711, 2012.

**Ćalić**, J.: Karstic uvala revisited: Toward a redefinition of the term, *Geomorphology*, 134, 32–42, doi:10.1016/j.geomorph.2011.06.029, 2011.

640 **Charrach**, J.: Investigations into the Holocene geology of the Dead Sea basin, *Carbonates and Evaporites*, 1–28, doi:10.1007/s13146-018-0454-x, 2018.

**Closson**, D.: Structural control of sinkholes and subsidence hazards along the Jordanian Dead Sea coast, *Environ. Geol.*, 47, 290–301, doi:10.1007/s00254-004-1155-4, 2005.

645 **Closson**, D. and **Abou Karaki**, N.: Sinkhole hazards prediction at Ghor Al Haditha, Dead Sea, Jordan: “Salt Edge” and “Tectonic” models contribution—a rebuttal to “Geophysical prediction and following development sinkholes in two Dead Sea areas, Israel and Jordan, by: Ezersky, M.G., Eppelbaum, L.V., Al-Zoubi, A.3, Keydar S., Abueladas, A-R., Akkawi E., and Medvedev, B.,” *Environ. Earth Sci.*, 70(6), 2919–2922, doi:10.1007/s12665-013-2418-8, 2013.

650 **Closson**, D. and **Karaki**, N. A.: Salt karst and tectonics : sinkholes development along tension cracks between parallel strike-slip faults , Dead Sea , Jordan, *Earth Surf. Process. Landforms* , 34(June), 1408–1421, doi:10.1002/esp, 2009.


**Cvijić**, J.: *Geomorfologija 2 (Geomorphology 2)*, 1926.

**Doğan**, U. and Özel, S.: Gypsum karst and its evolution east of Hafik (Sivas, Turkey), *Geomorphology*, 71, 373–388, doi:10.1016/j.geomorph.2005.04.009, 2005.

655 **Doğan**, U.: Land subsidence and caprock dolines caused by subsurface gypsum dissolution and the effect of subsidence on the fluvial system in the Upper Tigris Basin (between Bismil-Batman, Turkey), *Geomorphology*, 71(3–4), 389–401, doi:10.1016/j.geomorph.2005.04.010, 2005.

- El-Isa**, Z., Rimawi, O., Jarrar, G., Abou Karaki, N., Taqieddin, S., Atallah, M., Seif El-Din, N. and Al Saed, E.: Assessment of the Hazard of Sinkholes and Subsidence in the Ghor al-Haditha Area, Amman, Jordan., 1995.
- 660 **Ezersky**, M. G., Eppelbaum, L. V., Al-Zoubi, A., Keydar, S., Abueladas, A., Akkawi, E. and Medvedev, B.: Geophysical prediction and following development sinkholes in two Dead Sea areas, Israel and Jordan, *Environ. Earth Sci.*, 70(4), 1463–1478, doi:10.1007/s12665-013-2233-2, 2013.
- Fiaschi**, S., Closson, D., Abou Karaki, N., Pasquali, P., Riccardi, P. and Floris, M.: The complex karst dynamics of the Lisan Peninsula revealed by 25 years of DInSAR observations. Dead Sea, Jordan, *ISPRS J. Photogramm. Remote Sens.*, 130, 358–369, doi:10.1016/j.isprsjprs.2017.06.008, 2017.
- 665 **Filin**, S., Baruch, A., Avni, Y. and Marco, S.: Sinkhole characterization in the Dead Sea area using airborne laser scanning , 1135–1154, doi:10.1007/s11069-011-9718-7, 2011.
- Frumkin**, A.: Salt Karst, in *Treatise on Geomorphology*, vol. 6, edited by J. Shroder and A. Frumkin, pp. 407–424, Academic Press, San Diego, CA., 2013.
- 670 **Frumkin**, A. and Raz, E.: Collapse and subsidence associated with salt karstification along the Dead Sea, *Carbonates and Evaporites*, 16(2), 117–130, doi:10.1007/BF03175830, 2001.
- Frumkin**, A., Ezersky, M., Al-Zoubi, A., Akkawi, E. and Abueladas, A.-R.: The Dead Sea sinkhole hazard: Geophysical assessment of salt dissolution and collapse, *Geomorphology*, 134(1–2), 102–117, doi:10.1016/j.geomorph.2011.04.023, 2011.
- 675 **Garfunkel**, Z. and Ben-Avraham, Z.: The structure of the Dead Sea basin, *Tectonophysics*, 266(1–4), 155–176, doi:10.1016/S0040-1951(96)00188-6, 1996.
- GDAL/OGR Contributors**: GDAL/OGR Geospatial Data Abstraction software Library, Open Source Geospatial Found., 2018.
- Gutiérrez**, F. and Cooper, A. H.: Surface Morphology of Gypsum Karst, in *Treatise on Geomorphology*, vol. 6, edited by J. Shroder and A. Frumkin, pp. 425–437, Academic Press, San Diego, CA., 2013.
- 680 **Israel** Oceanographic and Limnological Research - Israel Marine Data Center: Interannual changes in the Dead Sea Total Vertical Stability and Sea Level, Long-Term Chang. Dead Sea [online] Available from: <https://isramar.ocean.org.il/isramar2009/DeadSea/LongTerm.aspx> (Accessed 10 February 2018), 2017.
- Khalil**, B.: The Geology of the Ar Rabba area, Map Sheet No 3125 IV, Bull 22, Amman, Jordan., 1992.




685 Kottmeier , Agnon, A., Al-halbouni, D., Alpert, P., Corsmeier, U., Dahm, T., Eshel, A., Geyer, S.,  
Haas, M., Holohan, E., Kalthoff, N., Kishcha, P., Krawczyk, C., Lati, J., Laronne, J. B., Lott, F., Mallast,  
U., Merz, R., Metzger, J., Mohsen, A., Morin, E., Nied, M., Rödiger, T., Salameh, E., Sawarieh, A.,  
Shannak, B., Siebert, C. and Weber, M.: New perspectives on interdisciplinary earth science at the Dead  
Sea: The DESERVE project, *Sci. Total Environ.*, 544(December 2015), 1045–1058,  
690 doi:10.1016/j.scitotenv.2015.12.003, 2016.

**Kranjc**, A.: Classification of Closed Depressions in Carbonate Karst, in *Treatise on Geomorphology*,  
Volume 6, edited by A. Frumkin, pp. 104–111, Academic Press, San Diego, CA, San Diego., 2013.

**Lensky**, N. G., Dvorkin, Y., Lyakhovsky, V., Gertman, I. and Gavrieli, I.: Water, salt, and energy balances  
of the Dead Sea, *Water Resour. Res.*, 41(12), doi:10.1029/2005WR004084, 2005.


695 **Lowe**, D. and Waltham, T.: A dictionary of karst and caves. *Cave Studies Series*, 6, British Cave Research  
Association, London., 1995.

**Meqbel**, N. M. M., Ritter, O. and Group, D.: A magnetotelluric transect across the dead sea basin:  
Electrical properties of geological and hydrological units of the upper crust, *Geophys. J. Int.*, 193(3),  
1415–1431, doi:10.1093/gji/ggt051, 2013. 

700 Monroe, W. H.: A glossary of karst terminology., 1970.

**Nof**, R., Abelson, M., Raz, E., Magen, Y., Atzori, S., Salvi, S., Baer, G., Nof, R. N., Abelson, M., Raz,  
E., Magen, Y., Atzori, S., Salvi, S. and Baer, G.: SAR Interferometry for Sinkhole Early Warning and  
Susceptibility Assessment along the Dead Sea, Israel, *Remote Sens.*, 11(1), 89, doi:10.3390/rs11010089,  
2019.

705 **Polom**, U., Alrshdan, H., Al-Halbouni, D., Holohan, E. P., Dahm, T., Sawarieh, A., Atallah, M. Y. and  
Krawczyk, C. M.: Shear wave reflection seismic yields subsurface dissolution and subsrosion patterns:  
application to the Ghor Al-Haditha sinkhole site, Dead Sea, Jordan, *Solid Earth*, 9, 1079–1098,  
doi:10.5194/se-9-1079-2018, 2018.

**Salameh**, E. and El-Naser, H.: Changes in the Dead Sea Level and their Impacts on the Surrounding  
710 Groundwater Bodies, *Acta Hydrochim. Hydrobiol.*, 28(1), 24–33, doi:10.1002/(SICI)1521-  
401X(200001)28:1<24::AID-AHEH24>3.0.CO;2-6, 2000. 

**Sauro**, U.: Closed Depressions in Karst Areas, in *Encyclopedia of Caves*, pp. 140–155., 2012.

- Sawarieh, A., Al Addas, A., Al Bashish, M. and Al Seba'i, E.: Sinkholes Phenomena At Ghor Al Haditha Study Area.- Internal Report No. 12, Amman, Jordan., 2000.
- 715 Shalev, E. and Lyakhovsky, V.: Viscoelastic damage modeling of sinkhole formation, *J. Struct. Geol.*, 42, 163–170, doi:10.1016/j.jsg.2012.05.010, 2012.
- Torfstein, A., Haase-Schramm, A., Waldmann, N., Kolodny, Y. and Stein, M.: U-series and oxygen isotope chronology of the mid-Pleistocene Lake Amora (Dead Sea basin), *Geochim. Cosmochim. Acta*, 73(9), 2603–2630, doi:10.1016/J.GCA.2009.02.010, 2009.
- 720 Waltham, T.: Large collapse sinkholes, old and new, in the Obruk Plateau, Turkey, *Cave Karst Sci.*, 42(3), 125–130, 2015.
- Yecheieli, Y.: Fresh-Saline Ground Water Interface in the Western Dead Sea Area, *Ground Water*, 38(4), 615–623, doi:10.1111/j.1745-6584.2000.tb00253.x, 2000.
- Yecheieli, Y. and Gavrieli, I.: Will the Dead Sea die?, *Geology*, 26(8), 755–758, doi:10.1130/0091-7613(1998)026<0755:WTDS>2.3.CO;2, 1998.
- 725 Yecheieli, Y., Abelson, M., Bein, A., Crouvi, O. and Shtivelman, V.: Sinkhole “swarms” along the Dead Sea coast: Reflection of disturbance of lake and adjacent groundwater systems, *Bull. Geol. Soc. Am.*, 118(9–10), 1075–1087, doi:10.1130/B25880.1, 2006.
- Yecheieli, Y., Kafri, U., Wollman, S., Shalev, E. and Lyakhovsky, V.: The effect of base level changes and geological structures on the location of the groundwater divide, as exhibited in the hydrological system between the Dead Sea and the Mediterranean Sea, *J. Hydrol.*, 378(3–4), 218–229, doi:10.1016/J.JHYDROL.2009.09.023, 2009.
- 730 Yecheieli, Y., Abelson, M. and Baer, G.: Sinkhole formation and subsidence along the Dead Sea coast, Israel, *Hydrogeol. J.*, 24(3), 601–612, doi:10.1007/s10040-015-1338-y, 2015.
- 735 Youssef, A. M., Al-Harbi, H. M., Gutiérrez, F., Zabramwi, Y. A., Bulkhi, A. B., Zahrani, S. A., Bahamil, A. M., Zahrani, A. J., Otaibi, Z. A. and El-Haddad, B. A.: Natural and human-induced sinkhole hazards in Saudi Arabia: distribution, investigation, causes and impacts, *Hydrogeol. J.*, 24(3), 625–644, doi:10.1007/s10040-015-1336-0, 2015.